Fermi surface in $LaRhSi_3$ and $CeRhSi_3$

T. Terashima（寺嶋太一), M. Kimata（木俣基), and S. Uji（宇治進也)
National Institute for Materials Science, Tsukuba, Ibaraki 305-0003, Japan

T. Sugawara（菅原徹也), N. Kimura（木村憲彰), and H. Aoki（青木晴善)
Center for Low Temperature Science, Tohoku University, Sendai, Miyagi 980-8578, Japan

H. Harima（播磨尚朝)
Department of Physics, Graduate School of Science, Kobe University, Kobe, Hyogo 657-8501, Japan
(Received 14 July 2008; revised manuscript received 16 September 2008; published 7 November 2008)

We report on de Haas-van Alphen (dHvA) effect measurements at ambient pressure and band-structure calculations for $LaRhSi_3$ and $CeRhSi_3$, whose crystal structures lack space-inversion symmetry. For $LaRhSi_3$, dHvA frequencies up to ~11 kT with effective masses up to $\sim 1.6m_e$, where m_e is the free-electron mass, are observed. The observed and the calculated Fermi surfaces are in satisfactory quantitative agreement. The energy splitting of bands due to the spin-orbit coupling is estimated to be of the order of 10^2 K. For $CeRhSi_3$, dHvA frequencies up to ~12 kT with effective masses up to $\sim 19m_e$ are observed. The dHvA frequency branches are definitely different from those observed in $LaRhSi_3$ and are difficult to explain with the $LaRhSi_3$ Fermi surface. This leads to the conclusion that the Ce $4f$ electrons in $CeRhSi_3$ are itinerant in the antiferromagnetic state at ambient pressure. The Fermi surface resulting from a band-structure calculation in which the Ce $4f$ electrons are treated as itinerant can provide a plausible explanation for the observed frequency branches, although the quantitative agreement is rather limited. The comparison of the calculated density of states with the Sommerfeld coefficient gives the mass enhancement factor of 8.

DOI: 10.1103/PhysRevB.78.205107 PACS number(s): 71.18.+y, 71.27.+a, 74.70.Tx

I. INTRODUCTION

$CeRhSi_3$ crystallizes in a tetragonal structure with the space group $I4mm$ (No. 107),[1–3] which lacks space-inversion symmetry. It orders antiferromagnetically with an incommensurate wave vector at the Néel temperature of $T_N = 1.6$ K at ambient pressure.[4,5] The small ordered moment of $\sim 0.1\mu_B$ is aligned in the c plane. It is a moderately heavy fermion with the Sommerfeld coefficient of $\gamma = 110$ mJ/mol K^2 measured in the antiferromagnetic state.[6] As pressure P is applied, T_N first goes up and then decreases for $P \gtrsim 8$ kbar.[7] Superconductivity emerges under pressure.[7] The superconducting transition temperature T_{sc} increases with pressure and becomes comparable to T_N at ~24 kbar.[7,8] T_{sc} peaks at 1.1 K near 26 kbar, and the initial slope of the upper critical field vs temperature curve, i.e., $-dB_{c2}/dT|_{T_{sc}}$, for the field B parallel to the c axis takes a maximum at the same pressure.[8] This strongly suggests that the antiferromagnetic phase terminates at this pressure. The upper critical field B_{c2} for $B \| c$ is anomalously large; $B_{c2}(0)$ at 29 kbar may reach 30 T.[8] Intriguing superconducting properties of $CeRhSi_3$ (see Ref. 9 for a brief review) have been stimulating theoretical studies[10–18] on noncentrosymmetric superconductivity originally initiated by $CePt_3Si$.[19] Subsequent to $CeRhSi_3$, superconductivity has also been found in the Ir-substituted compound $CeIrSi_3$.[20]

We here concentrate on the Fermi surface. The initial de Haas-van Alphen (dHvA) effect study showed that dHvA frequency branches in $CeRhSi_3$ were very different from ones in $LaRhSi_3$.[21] This strongly suggests that the Fermi surface in $CeRhSi_3$ is different from that in $LaRhSi_3$ most likely because of the participation of the Ce $4f$ electrons in the Fermi surface (La is next to Ce in the periodic table and has no f electron). A recent dHvA study under high pressure has shown that the Fermi surface and effective masses of electrons in $CeRhSi_3$ evolve continuously with pressure up to 30 kbar, exhibiting no jump as a function of pressure.[22] This is in sharp contrast to what was observed in $CeRhIn_5$[23] in which it is believed that the Ce $4f$ electrons transform from localized to itinerant as the antiferromagnetism disappears with pressure. It is, on the other hand, exactly the behavior expected when the Ce $4f$ electrons are itinerant already in the antiferromagnetic phase. Whether the Ce $4f$ electrons are localized or itinerant in antiferromagnetic phases of heavy fermions is the key to the nature of the heavy fermion quantum criticality and hence is one of current focuses of researches in this area.[24,25] In this paper, we perform dHvA measurements on $CeRhSi_3$ and $LaRhSi_3$ and also band-structure calculations for them. We will present further evidence that the Ce $4f$ electrons in $CeRhSi_3$ are itinerant in the antiferromagnetic phase at ambient pressure.

II. EXPERIMENTS AND BAND-STRUCTURE CALCULATIONS

Single crystals of $LaRhSi_3$ and $CeRhSi_3$ were grown by the Czochralski method as described in Ref. 21. Residual resistivity ratios larger than 100 were observed in grown crystals, indicating their high quality.

dHvA oscillations were measured in a top-loading dilution refrigerator (base temperature: ~35 mK) equipped with a 20 T superconducting magnet. The field-modulation technique was employed,[26] and the detection was made at the second harmonic of the modulation frequency. Most mea-

surements were carried out with a modulation frequency of 67 Hz and an amplitude of 0.01 T, but for the determination of effective masses in $CeRhSi_3$ a smaller frequency of 17 Hz or a smaller amplitude of 0.004 T were chosen to reduce eddy-current heating of a sample. For angular studies, a sample placed in a pickup coil was rotated together with the pickup coil. We basically performed two field sweeps at each field direction: one from $B=7$ to 13.9 T and the other from 14 to 17.5 T. In the case of $LaRhSi_3$, one crystal was used throughout. Its c axis was set parallel to the pickup coil axis for measurements in the (010) plane, while its a axis was set parallel to the coil axis for measurements in the (001) plane. In the case of $CeRhSi_3$, two crystals were used for measurements in different planes: one was used for (010)-plane measurements with its c axis parallel to the coil axis, while the other was used for (001)-plane measurements with its a axis parallel to the coil axis. Effective masses (m^*) and Dingle temperatures (x_D^*) associated with dHvA frequencies (F) were determined from temperature and field dependences of dHvA oscillation amplitudes as usual,[26] and electron mean-free paths (l) were calculated from observed F, m^*, and x_D^*. The temperature ranges used for the mass determinations were up to ~2 K for $LaRhSi_3$ and ~0.2 K for $CeRhSi_3$. The same experimental setup as the dHvA one can be used to measure ac magnetic susceptibility.

The electronic band structures of $LaRhSi_3$ and $CeRhSi_3$ were calculated by using a full potential linearized augmented plane wave (FLAPW) method with the local-density approximation (LDA) for the exchange-correlation potential. We used the program codes TSPACE (Ref. 27) and KANSAI-03. The scalar relativistic effects were taken into account for all electrons, and the spin-orbit interactions were included self-consistently for all valence electrons in a second variational procedure. For $LaRhSi_3$, the unoccupied $4f$ levels of La were shifted upward by 0.2 Ry by hand to improve the agreement between the calculated and the experimental Fermi surfaces.[28,29]

The lattice parameters used for the calculations were $a=4.277$ Å and $c=9.760$ Å for $LaRhSi_3$ and $a=4.237$ Å and $c=9.785$ Å for $CeRhSi_3$.[30] The atomic coordinates were assumed to be the same as those in $LaIrSi_3$ (Ref. 2): La or Ce (2a site) being at the origin, $z=0.6553$ for the 2a sites of Ir, $z=0.4112$ for the 2a sites of Si(1), and $z=0.2615$ for the 4b sites of Si(2). The muffin-tin (MT) radii were set as $0.3603a$ for La or Ce and $0.2478a$ for Rh and Si. Core electrons (Kr core plus $4d^{10}$ for La and Ce, Ar core plus $3d^{10}$ for Rh, and Ne core for Si) were calculated inside the MT spheres in each self-consistent step. The $5s^25p^6$ electrons on La or Ce and the $4s^24p^6$ electrons on Rh were treated as valence electrons by using a second energy window. Note that in the calculation for $CeRhSi_3$ a paramagnetic state was assumed and the $4f$ electrons of Ce were treated as itinerant. Hence $CeRhSi_3$ is an uncompensated metal, whereas $LaRhSi_3$ is a compensated metal.

The LAPW basis functions were truncated at $|\mathbf{k}+\mathbf{G}_i| \leq 5.1\times 2\pi/a$, corresponding to 615 LAPW functions at the Γ point. The sampling points were uniformly distributed in the irreducible (1/8)th of the Brillouin zone (IBZ); 369 $\mathbf{k}$ points (divided by 16,16,8) were used both for the potential convergence and for the final band structure. Note that be-

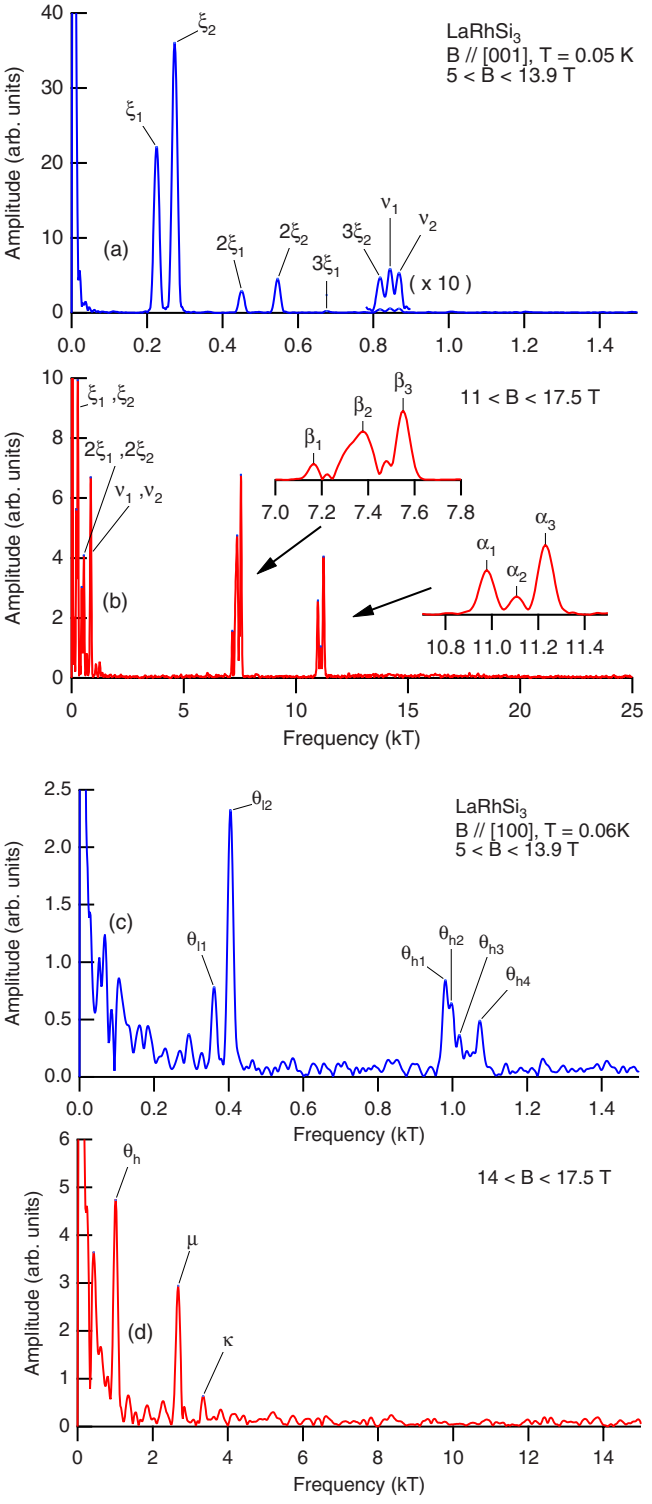

FIG. 1. (Color online) Fourier spectra of dHvA oscillations in $LaRhSi_3$ for [(a) and (b)] $B\|[001]$ and [(c) and (d)] $B\|[100]$. For each field direction, low-field and high-field data are shown. For $B\|[001]$, the field range of the high-field sweep ($11<B<17.5$ T) was made longer than usual ($14<B<17.5$ T) to resolve closely spaced frequencies. Fundamental frequencies are labeled with Greek letters and "2ξ," "3ξ," etc., indicate the second and the third harmonics of ξ and so on.

TABLE I. Experimental and calculated Fermi-surface parameters of $LaRhSi_3$.

Field direction	Experiment					Calculation			
	Branch	F (kT)	m^*/m_e	x_D^* (K)	l (μm)	Orbit[a]	F (kT)	$m_{\rm band}/m_e$	$m^*/m_{\rm band}$
[001]	ξ_1	0.23	0.23(2)	4.2(5)	0.119(3)	Γ_{39}^h	0.27	0.14	1.6
	ξ_2	0.27	0.23(2)	4.4(5)	0.127(3)	Γ_{40}^h	0.31	0.15	1.5
	(θ)					F_{38}^h	0.31	0.52	
	ν_1	0.84	~0.6			Γ_{41}^h	0.90	0.41	~1.5
	ν_2	0.87	~0.6			Γ_{42}^h	0.95	0.44	~1.4
	β_1	7.17				Z_{39}^h	7.38	0.92	
						Λ_{39}^h	7.53	1.58	
	β_2	7.38	1.25(5)			Z_{40}^h	7.75	0.99	1.3
	β_3	7.55	1.18(4)	6(2)	0.09(2)	Λ_{40}^h	8.01	1.20	0.98
	α_1	10.98	1.47(5)	3.8(8)	0.15(3)	Γ_{42}^e	10.72	1.03	1.4
	α_2	11.11							
	α_3	11.23	1.46(5)	4.3(6)	0.13(1)	Γ_{41}^e	11.00	1.00	1.5
[100]	θ_{l1}	0.36	0.46(5)			(F_{38}^h	0.29	0.44	1.1)
	θ_{l2}	0.41	0.37(2)	7.3(7)	0.057(3)	F_{38}^h	0.29	0.44	0.91
	θ_{h1}	0.98	0.57(3)			F_{38}^h	1.00	0.79	0.72
	θ_{h2}	1.00	0.45(3)			(F_{38}^h	1.00	0.79	0.57)
	θ_{h3}	1.02				(F_{38}^h	1.00	0.79)	
	θ_{h4}	1.07	0.70(4)			(F_{38}^h	1.00	0.79	0.89)
	μ	2.68	0.92(8)	6.7(8)	0.065(3)	Σ_{42}^e	2.65	0.69	1.3
						Σ_{41}^e	2.95	1.13	
						Σ_{42}^e	2.98	0.67	
	κ	3.34	1.1(1)			Σ_{41}^e	3.21	0.67	1.6
						Σ_{41}^e	5.19	2.02	
[110][b]	θ_1	0.50				gp_{38}^h	0.43	0.60	
	θ_2	0.53				(gp_{38}^h	0.43	0.60)	
	θ_3	0.55				(gp_{38}^h	0.43	0.60)	
	θ_4	0.57				(gp_{38}^h	0.43	0.60)	
	θ_5	0.59				(gp_{38}^h	0.43	0.60)	
	ϕ_1	0.81				Δ_{42}^e	0.73	0.61	
	ϕ_2	0.82				Δ_{41}^e	0.77	0.65	
	ζ_1	6.53				Δ_{42}^e	6.14	1.33	
	ζ_2	7.05				Δ_{41}^e	6.61	1.43	

[a]The orbit assignments are denoted by orbit center, band number, and orbit character, i.e., electron or hole. "gp" is an abbreviation for a general point.
[b]The experimental data for $B\|[110]$ are from Ref. 9.

cause of the space-group symmetry, all electronic bands remain doubly degenerate along the Λ line in the Brillouin zone.

III. RESULTS AND DISCUSSION

A. $LaRhSi_3$

Figure 1 shows Fourier spectra of dHvA oscillations in $LaRhSi_3$ for $B\|[001]$ and $B\|[100]$. The spectra of the low-field sweeps have a higher frequency resolution because of the wider $1/B$ range used, and also low-frequency oscillations are generally easier to see in low-field regions because of the experimental Bessel factor.[26,31] On the other, the high-field spectra show high-frequency oscillations more clearly. Most of the frequencies appear as doublets or multiplets. We basically follow Ref. 9 in labeling the frequencies; however, the frequencies λ_2, λ_1, and ϵ_2 in Ref. 9 are renamed as ξ_1, ξ_2, and ν, and the frequency ϵ_1 is assigned to the second harmonic of ν. Table I lists the frequencies, associated effective masses, Dingle temperatures, and mean-free paths. Table I also shows dHvA frequencies for $B\|[110]$ taken from Ref. 9. The angular dependence of dHvA frequencies are depicted in Fig. 2; both low-field and high-field data are shown together. The frequency branches α, β, ν, ξ, κ, and θ are noticeable.

The data in the $(1\bar{1}0)$ plane are taken from Ref. 9. Since a different sample was used in Ref. 9, the [110]-axis data on the left side of Fig. 2 (taken from Ref. 9) differ from those on the right side (from present measurements). The fact that a larger number of frequencies has been observed in Ref. 9 may suggest that the sample of Ref. 9 is better than the present one. For the [001] direction, there is a much better correspondence between the present data and those in Ref. 9 except that the θ frequencies are not observed for this field direction in the present measurements.

Figures 3(a) and 3(b) show calculated energy-band structure and total and partial densities of states of $LaRhSi_3$. The density of states at the Fermi level is estimated at 23.9 states/Ry f.u. This corresponds to the Sommerfeld coefficient of $\gamma=4.13$ mJ/mol K^2, which is compared with the experimental value of $\gamma=5.1$ mJ/mol K^2.[30] The partial densities of states indicate that the La d, Rh d, and Si p states contribute to energy bands near the Fermi level but that the sum of these partial densities of states accounts for less than half of the total density of states. Hence, conduction electrons are extended well to the interstitial region. Six bands, 37–42, cross the Fermi level, although band 37 does not cross the Fermi level along the symmetry lines shown in Fig. 3(a). The resultant Fermi surface, consisting of three pairs of inversion-asymmetry-split sheets, is shown in Fig. 3(c), where some of possible extremal cyclotron orbits are indicated. Theoretical dHvA frequencies predicted by this Fermi surface are shown in Fig. 2 and Table I. In the latter, calculated band masses (m_{band}) are also listed. Low frequency branches ($F \lesssim 100$ T) due to band-37 hole surface are neglected.

By comparing the experimental and theoretical frequencies (Fig. 2), we can identify cyclotron orbits responsible for the frequency branches α, β, ξ, κ, μ, and θ as shown in Fig. 3(c). Although not shown in the figure, orbits for the ν, ζ, and ϕ branches are found on the band-41 and -42 electron surfaces. ν is assigned to a Γ-centered orbit circuiting the interior of the surfaces, ζ to an orbit centered at a point on the [110] line traversing two of the four lobes of the surfaces, and ϕ to an orbit around a thin part between the lobes of the surfaces centered at a point on the $[1\bar{1}0]$ line. Frequencies between ~1 and ~5 kT observed near [110] in the $(1\bar{1}0)$ plane are probably harmonics of the θ frequencies. Their oscillation amplitudes decrease approximately but not exactly exponentially with the harmonic number. This is a characteristic of harmonics when the spin-splitting factor is not negligible, i.e., both spins contribute to dHvA oscillations.[26] The α and θ branches exhibit finer splitting than theoretically expected. In the case of α, we assume that α_1 and α_3 are ascribable to Fermi surfaces 41 and 42, respectively. The origin of α_2, in the middle of the two, is not clear at present, but this might possibly be explained by magnetic breakdown between the two orbits. Regarding the splitting of θ, a possible explanation is that band-37 hole surface is larger than calculation and support an orbit similar to θ. This can explain well the doublet structure of θ_l in the (001) plane. However, the finer splitting of θ_h and especially that of θ in the $(1\bar{1}0)$ plane need some more reasons; magnetic breakdown may need to be involved.

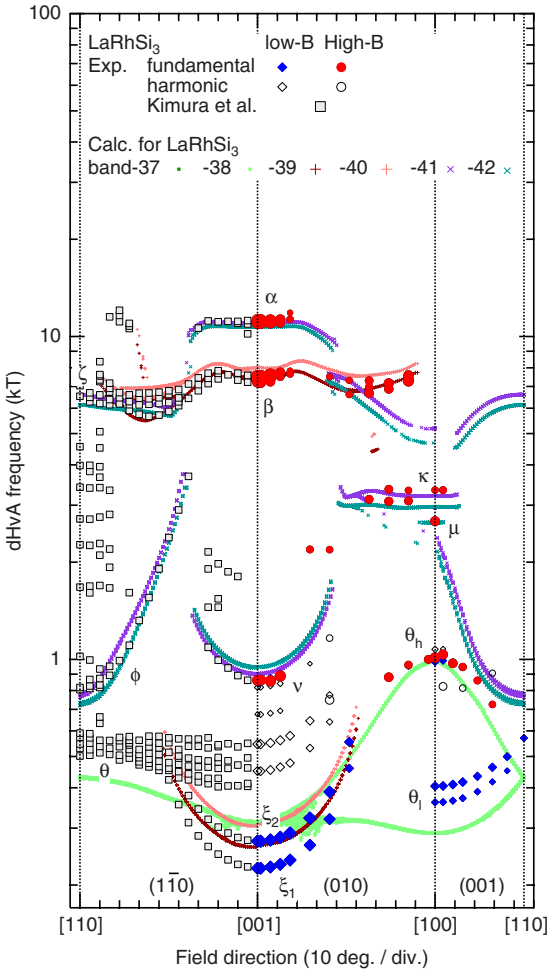

FIG. 2. (Color online) Angular dependence of dHvA frequencies in $LaRhSi_3$. The circles and diamonds denote experimental frequencies determined from the high-field ($14<B<17.5$ T) and the low-field ($7<B<13.9$ T) sweeps, respectively. Frequencies ascribed to harmonics are shown by open symbols. The sizes of the symbols are based on the amplitudes of dHvA oscillations. The squares in the $(1\bar{1}0)$ plane are data points by Kimura *et al.* (Ref. 9). The Greek letters indicate the names of frequency branches. The dots and small + and × marks show frequencies predicted by the band-structure calculation, which yields the Fermi surface shown in Fig. 3(c). Low-frequency branches ($F \lesssim 100$ T) due to band-37 hole surface are neglected.

We can estimate the strength of the spin-orbit coupling from the inversion-asymmetry splitting of dHvA frequencies. We follow the notation of Ref. 32. The spin-orbit coupling in a noncentrosymmetric crystal splits a doubly degenerated unperturbed energy band $\epsilon_0(\mathbf{k})$ into two: $\epsilon_\lambda(\mathbf{k})=\epsilon_0(\mathbf{k})+\lambda|\boldsymbol{\alpha}(\mathbf{k})|$, where $\lambda=\pm$ is the band index. Assuming the Rashba model,[33] $\boldsymbol{\alpha}(\mathbf{k})=\alpha_\perp(k_y\hat{\mathbf{x}}-k_x\hat{\mathbf{y}})$. The energy splitting of the two bands $2|\alpha_\perp|k_F$ is related to the splitting of the dHvA frequencies ΔF for $B\|[001]$ as $2|\alpha_\perp|k_F=(\hbar e/c)\Delta F/m_\perp$, where k_F and $m_\perp$ are the Fermi wave number and the effective mass in the (001) plane, respectively. From the frequency differences between α_1 and α_3, β_1 and β_2, ν_1 and ν_2, and ξ_1 and ξ_2, we obtain the energy splittings of $2|\alpha_\perp|k_F=2.3\times10^2$, 2.3×10^2, 54, and 2.8×10^2 K, respectively.

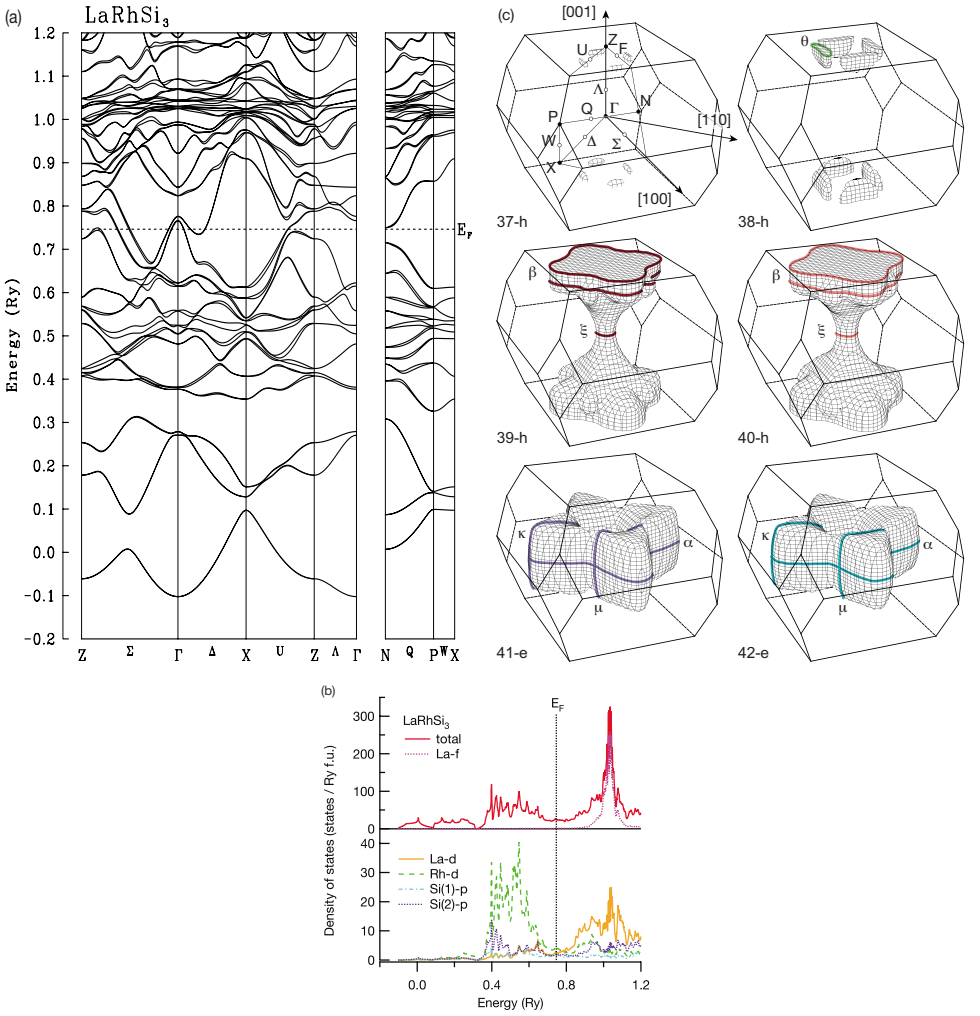

FIG. 3. (Color online) (a) Calculated electronic band structure along the high-symmetry directions near the Fermi level E_F, (b) total and partial densities of states, and (c) Fermi surface of $LaRhSi_3$. In the calculation, the unoccupied $4f$ levels of La were shifted upward by 0.2 Ry. The Fermi surface consists of band-37, -38, -39, and -40 hole surfaces and band-41 and -42 electron surfaces. Cyclotron orbits responsible for some of the dHvA frequency branches are also indicated. The points of symmetry (black circles) and the lines of symmetry (lines marked by white circles) in the Brillouin zone are explained in the top left figure of (c).

Here we have used the average of the two effective masses as $m_\perp$ for each pair except for β. For β, we have used the effective mass of β_2 since that of β_1 could not be determined (Table I).

$LaRhSi_3$, $LaIrSi_3$,[34] and $LaTGe_3$ (T=Co, Rh, and Ir)[35,36] have very similar Fermi surfaces. We here compare the Fermi surface of $LaRhSi_3$ with those of the two closest compounds $LaIrSi_3$ and $LaRhGe_3$. In the case of $LaIrSi_3$, band 37 does not cross the Fermi level and band 38 hole surface is smaller than the corresponding one in $LaRhSi_3$. On the other hand, in the case of $LaRhGe_3$, the four pieces of each of band-37(65) and -38(66) hole surfaces merge into one (the band numbers are different for $LaRhGe_3$, and the numbers in the parentheses refer to the band numbers for $LaRhGe_3$). For band-39(67) and -40(68) hole surfaces, the necks at Γ disappear in $LaIrSi_3$, and these surfaces become closed. In the case of $LaRhGe_3$, the necks barely remain but are very much thinner than those in $LaRhSi_3$. For band-41(69) and -42(70) electron surfaces, the basic shape, a tetragonally distorted torus, is the same for the three compounds, although details

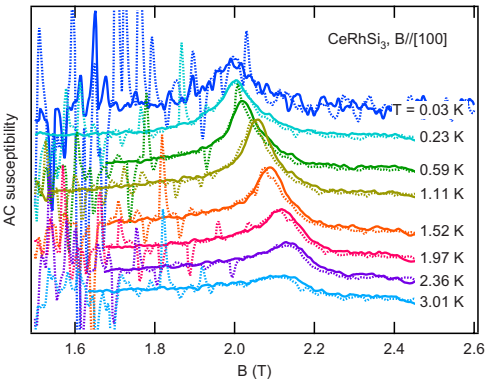

FIG. 4. (Color online) Magnetic-field dependence of ac magnetic susceptibility along the [100] direction in $CeRhSi_3$. The dotted and solid lines show up- and down-field data, respectively. The lines are vertically shifted for clarity. The measurement temperatures are indicated in the figure. Spike noises, especially frequent in the up-sweep data below 2 T, are due to flux jumps in the superconducting magnet and have nothing to do with the sample.

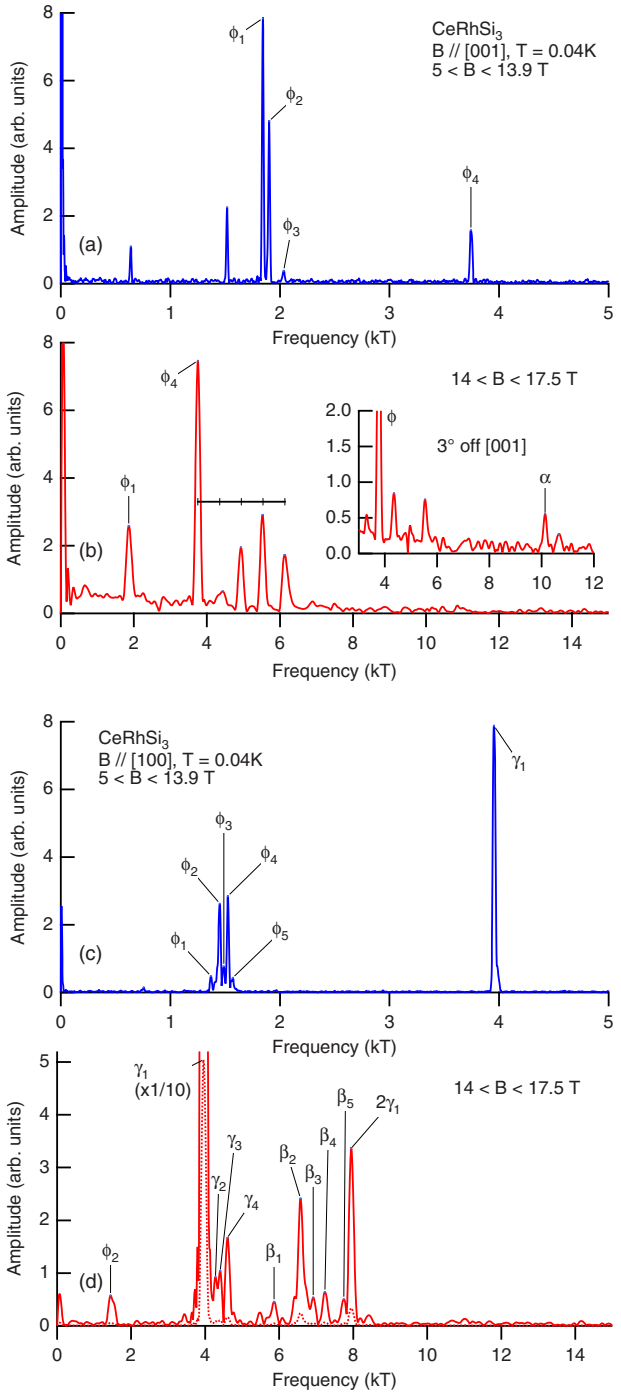

FIG. 5. (Color online) Fourier spectra of dHvA oscillations in $CeRhSi_3$ for [(a) and (b)] $B\|[001]$ and [(c) and (d)] $B\|[100]$. For each field direction, low-field and high-field data are shown. Some of the frequencies are labeled with Greek letters. The inset to (b) is a spectrum for a field direction of 3° off the [001] axis in the (010) plane to show the α frequency. The horizontal line with a scale in (b) indicates that ϕ_4 and the next four higher frequencies are almost equally spaced.

vary among them. The cross sections normal to [001] are smaller in $LaIrSi_3$ and $LaRhGe_3$ than in $LaRhSi_3$.

The inversion-asymmetry splitting of energy bands may also be compared with those found in analogous compounds.

TABLE II. Experimental Fermi-surface parameters of $CeRhSi_3$.

Field direction	Experiment				
	Branch	F (kT)	m^*/m_e	x_D^* (K)	l (μm)
[001]		0.64			
		1.52			
	ϕ_1	1.84	7.0(7)		
	ϕ_2	1.90			
	ϕ_3	2.04			
	ϕ_4	3.74	10.8(9)	0.18(3)	0.24(2)
		4.43			
		4.93			
		5.52	18.6(8)		
		6.13			
[100]		0.76			
	ϕ_1	1.37			
	ϕ_2	1.45	4.1(3)		
	ϕ_3	1.49			
	ϕ_4	1.53	5.8(2)		
	ϕ_5	1.57			
	γ_1	3.96	16.5(4)	0.087(7)	0.34(2)
	γ_2	4.28			
	γ_3	4.40			
	γ_4	4.60			
	β_1	5.86			
	β_2	6.58			
	β_3	6.92			
	β_4	7.24			
	β_5	7.75			
[110][a]		0.38			
		2.01			
		2.22			
		2.30			
		4.30			
	γ	4.95			
	ϵ	6.25			

[a]The experimental data for $B\|[110]$ are from Ref. 21.

In the order of $LaIrSi_3$ and $LaTGe_3$ (T=Co, Rh, and Ir),[34–36] $2|\alpha_\perp|k_F$=1100, 461, 511, and 1090 K for the α branches and $2|\alpha_\perp|k_F$=1250, 416, 505, and 1066 K for the β branches. The large splittings in the Ir compounds may be explained by the large atomic number of Ir and the large 5d-electron population close to the nucleus.[36] While the splittings are similar between $LaIrSi_3$ and $LaIrGe_3$, the splittings in $LaRhSi_3$ are less than half of those in $LaRhGe_3$. This difference can mainly be explained by the differences in the effective masses in the four compounds. Note that $2|\alpha_\perp|k_F$ is inversely proportional to $m_\perp$. While the relevant effective masses are 30%–40% smaller in $LaIrSi_3$ than in $LaIrGe_3$, they are 40%–50% larger in $LaRhSi_3$ than in $LaRhGe_3$.[34–36]

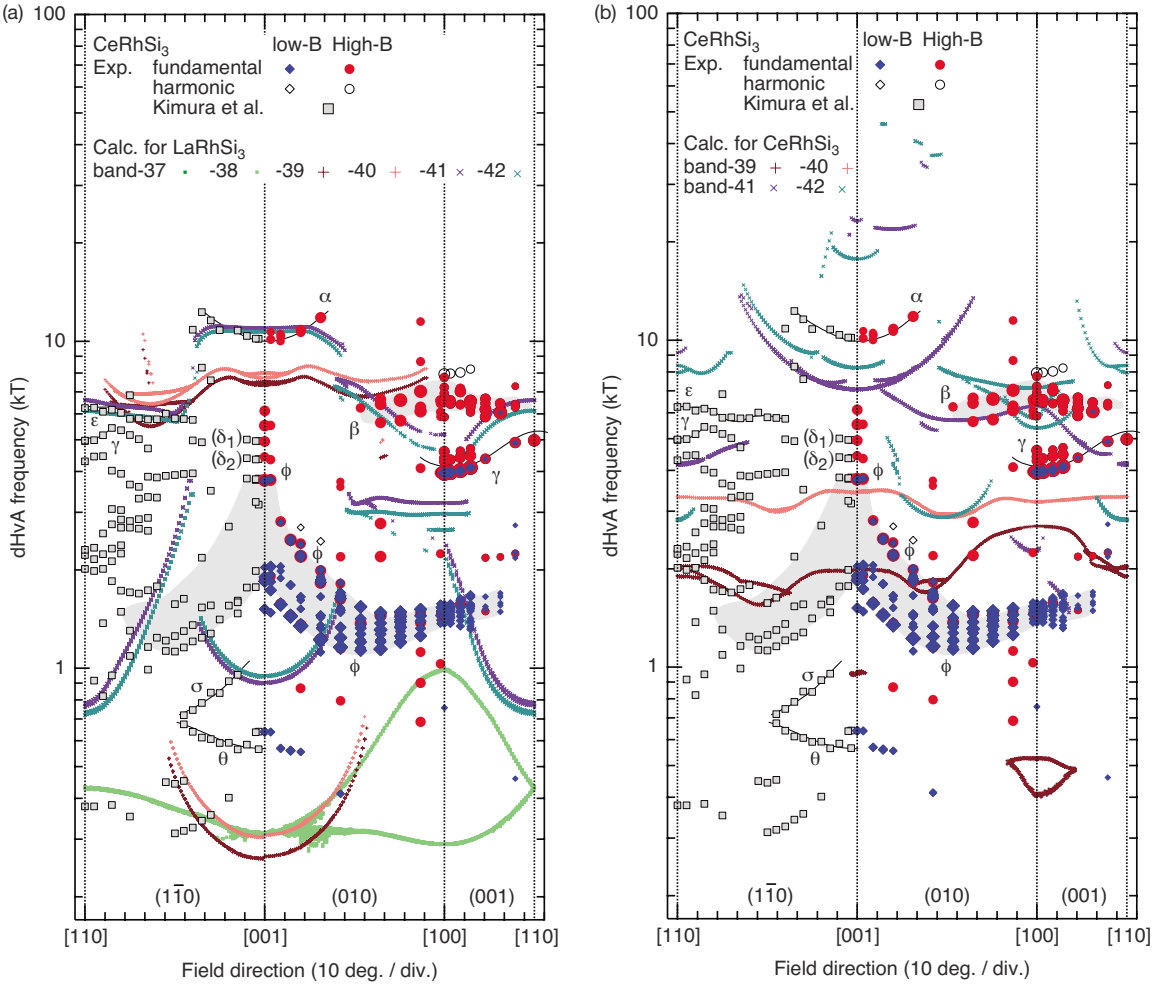

FIG. 6. (Color online) Angular dependence of dHvA frequencies in $CeRhSi_3$. The circles and diamonds denote experimental frequencies determined from the high-field ($14<B<17.5$ T) and the low-field ($7<B<13.9$ T) sweeps, respectively. Frequencies ascribed to harmonics are shown by open symbols. The sizes of the symbols are based on the amplitudes of dHvA oscillations. The squares in the $(1\bar{1}0)$ plane are data points by Kimura *et al.* (Ref. 21). The Greek letters indicate the names of frequency branches (or rather frequency bands in some cases), which are marked by thin lines or shadings. The dots and small + and × marks in (a) show frequencies predicted by the band-structure calculation for $LaRhSi_3$, which yields the Fermi surface shown in Fig. 3(c). On the other hand, the small + and × marks in (b) show frequencies predicted by the band-structure calculation for $CeRhSi_3$ with the itinerant $4f$ electrons, which yields the Fermi surface shown in Fig. 7(c).

B. $CeRhSi_3$

We first consider whether $CeRhSi_3$ remains in the antiferromagnetic state during dHvA measurements when magnetic fields up to 17.5 T are applied. Specific heat measurements have shown that T_N hardly changes even when 8 T is applied along the a or c axis.[6] ac susceptibilities measured up to 17.5 T along the a and c axes in the present study show no sign of a metamagnetic transition or an entrance to a paramagnetic state, i.e., a field-induced ferromagnetic state except for a tiny anomaly described below. Magnetization measurements at $T=1.85$ K ($>T_N$) show that magnetizations increase almost linearly up to 7 T for the a and c axes and that the induced moment is only about $0.1\mu_B$ ($0.04\mu_B$) for the a (c) axis even at 7 T.[9,30] This indicates that $CeRhSi_3$ is not easily polarized and is in line with the absence of a metamagnetic transition or field-induced ferromagnetic state up to 17.5 T. According to these observations, we can safely assume that the present dHvA measurements were performed in the antiferromagnetic state.

The above mentioned tiny anomaly in the ac susceptibility is found around 2 T for $B\|[100]$ (Fig. 4). The anomaly is observed not only below T_N but also above T_N. The susceptibility peak is largest and sharpest at around 1 K rather than at the lowest temperature. No clear hysteresis is observed. Since the present setup is not calibrated for susceptibility, the absolute values of the susceptibility peak heights are not known, but the observation that the heights are comparable to dHvA oscillation amplitudes at high fields indeed indicates that the anomaly is weak. The anomaly may be attributed to the rotation of the magnetic-moment direction in the c plane. It is interesting to note that $CeIrSi_3$ also exhibits a nonlinear magnetization curve for $B\|[100]$, although in this case the nonlinearity appears only below T_N.[34]

Figure 5 shows Fourier spectra of dHvA oscillations in $CeRhSi_3$ for $B\|[001]$ and $B\|[100]$. A spectrum for a field

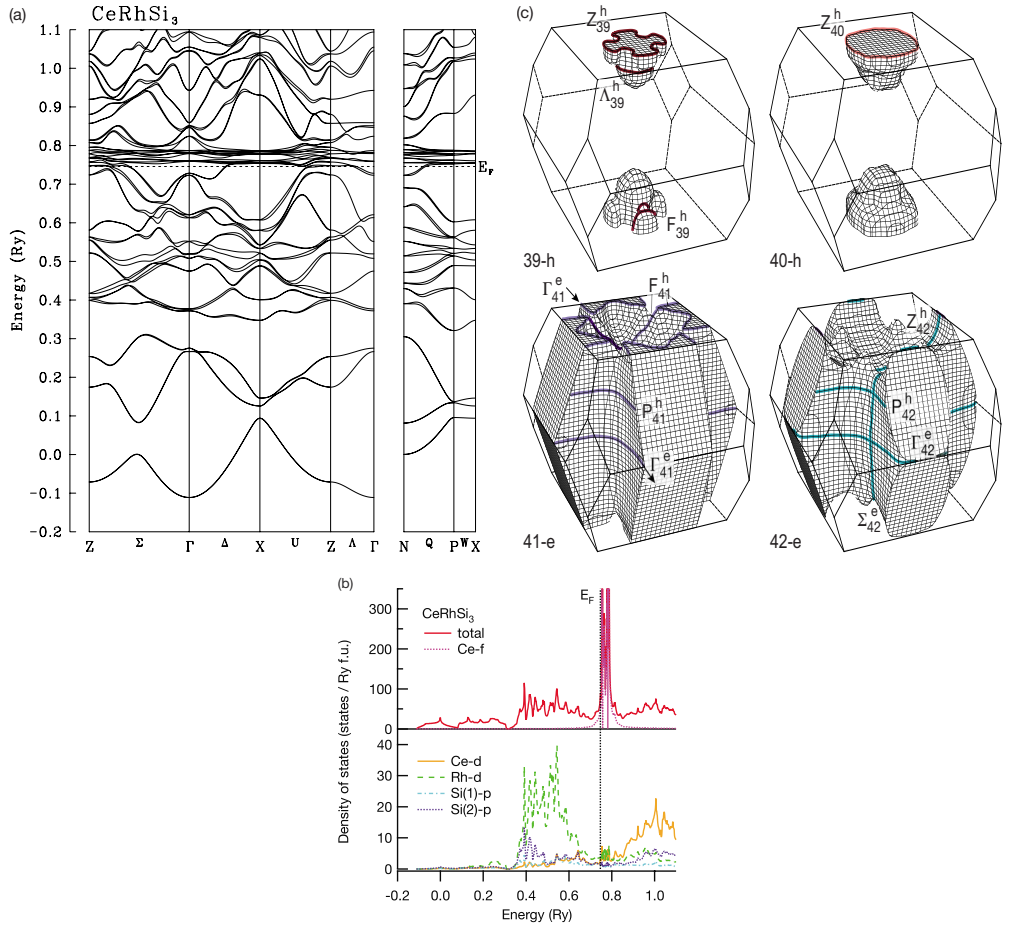

FIG. 7. (Color online) (a) Calculated electronic band structure along the high-symmetry directions near the Fermi level E_F, (b) total and partial densities of states, and (c) Fermi surface of $CeRhSi_3$. The Ce $4f$ electrons are assumed to be itinerant. The Fermi surface consists of band-39 and -40 hole surfaces and band-41 and -42 electron surfaces. Some of expected extremal orbits are indicated in (c).

direction of 3° off the [001] axis toward [100] is also shown in the inset to Fig. 5(b), where the α frequency can be seen. We basically follow Ref. 21 in labeling frequencies. We however rename δ_3 in Ref. 21 as ϕ_4 and regard δ_1 and δ_2 in Ref. 21 as arising from ϕ_4 owing to the magnetic breakdown or magnetic interaction effect. ϕ_4 and the next four higher frequencies are almost equally spaced [Fig. 5(b)], which strongly suggests that the magnetic breakdown or magnetic interaction effect is involved and δ_1 and δ_2 are the lowest two of the four frequencies. For the β and γ frequencies [Fig. 5(d)], we have given subscript numbers in ascending order of frequency as opposed to descending order in Ref. 21. Table II lists the frequencies, associated effective masses, Dingle temperatures, and mean-free paths. The frequencies for $B\|[110]$ are extracted from Ref. 21. For the effective masses, the magnetic-field dependence was examined for $B\|[100]$ but no appreciable dependence was found. The angular dependence of the frequencies is shown in Figs. 6(a) and 6(b). The theoretical frequencies calculated for $LaRhSi_3$ and those calculated for $CeRhSi_3$ with the itinerant Ce $4f$ electrons are shown in (a) and (b), respectively, for comparison. Note that the data points in the $(1\bar{1}0)$ plane are taken from Ref. 21 and that the three different samples were used for the three planes $(1\bar{1}0)$, (010), and (001). Because of the different samples, the [110]-axis data on the left sides of Figs. 6(a) and 6(b) (taken from Ref. 21) and those on the right sides (present measurements) are not identical. The fact that a larger number of frequencies has been observed in Ref. 21 may suggest that the sample of Ref. 21 is better than the present one used for the (001) plane. For the (010) plane, the present data resemble those in Ref. 21 more closely.

If the Ce $4f$ electrons in $CeRhSi_3$ are localized, the Fermi surface in a paramagnetic state of $CeRhSi_3$ will be essentially identical to that of $LaRhSi_3$. Since $CeRhSi_3$ orders antiferromagnetically at ambient pressure, the Fermi surface will be truncated by antiferromagnetic energy gaps. Those gaps are usually small and magnetic breakdown can occur. Therefore, in the antiferromagnetic state of $CeRhSi_3$, we will see two kinds of dHvA frequencies, i.e., frequencies that are essentially the same as ones in $LaRhSi_3$ and frequencies that are smaller than original ones in $LaRhSi_3$ because of the truncation. However, we cannot expect frequencies that are larger than the largest ones in $LaRhSi_3$. With this in mind, we compare Fig. 6(a) with Fig. 2. We can hardly see any resemblance between the frequency branches in $CeRhSi_3$ and those in $LaRhSi_3$. Although the α frequencies are similar in size between the two compounds, their angular dependences are quite different. While α in $LaRhSi_3$ is nearly constant for field directions near [001], α in $CeRhSi_3$ increases apprecia-

bly as the field is tilted from [001]. In addition, α in $CeRhSi_3$ is not observed when the field is aligned close enough to [001] [Fig. 5(b)] in contrast to α in $LaRhSi_3$. Thus the α branches have different origins in the two compounds. The frequencies β, ν, and ξ are observed clearly for field directions around [001] in $LaRhSi_3$, whereas no corresponding frequencies exist in $CeRhSi_3$. Further, the β frequencies observed near [100] in $CeRhSi_3$ are distinctly larger than the largest theoretical frequencies for those field directions in $LaRhSi_3$ ($F \sim 5.2$ kT from the Σ^e_{41} orbit; see Table I). They are difficult to explain with the Fermi surface of $LaRhSi_3$ and strongly suggest that the Fermi surface of $CeRhSi_3$ are larger including the Ce $4f$ electrons.

We now turn to the Fermi surface of $CeRhSi_3$ with the itinerant Ce $4f$ electrons. Figures 7(a) and 7(b) show energy-band structure and total and partial densities of states derived from the band-structure calculation. The total density of states at the Fermi level is 79.1 states/Ry f.u., corresponding to the Sommerfeld coefficient of $\gamma = 13.7$ mJ/mol K^2. By comparing this value with the experimental one of $\gamma = 110$ mJ/mol K^2 in the antiferromagnetic state,[6] we may deduce a moderately large specific-heat mass enhancement factor of 8. The partial densities of states indicate that electronic states near the Fermi level in $CeRhSi_3$ are predominantly of Ce $4f$ character; about 70% of the density of the states at the Fermi level is ascribed to the Ce $4f$ character. Four bands, 39–42, cross the Fermi level, resulting in the Fermi surface shown in Fig. 7(c), where some of expected extremal cyclotron orbits are indicated. Theoretical dHvA frequencies predicted by this Fermi-surface model are depicted in Fig. 6(b) and are listed together with calculated band masses for the symmetry directions in Table III. Because of the band degeneracy along the Λ line, hole surfaces 39 and 40 touch each other on the Λ line and hence a middle frequency may exist between frequencies due to orbits Z^h_{39} and Z^h_{40} for field directions in the (001) plane. The same argument can be applied to the pair of electron surfaces 41 and 42. However, those middle frequencies are not shown in Fig. 6(b) or Table III.

This Fermi-surface model [Fig. 7(c)] seems as a promising starting point for the real Fermi surface in $CeRhSi_3$. The α frequency may be attributed to the orbit P^h_{42} or P^h_{41} [see Fig. 6(b) together with Table III]. The β frequencies near [100] may be ascribed to the orbits Σ^e_{42}, F^h_{42}, Z^h_{41}, and Z^h_{42}. The ϕ frequencies might be explained by the orbits Z^h_{39} and Z^h_{40}, although surfaces 39 and 40 would have to be largely deformed to explain the ϕ frequencies near [100]. If we can assume that the frequencies ϕ_1 and ϕ_4 at [001] are inversion-asymmetry-split pairs, then the energy splitting will be estimated as $2|\alpha_\perp|k_F = 1.4 \times 10^2$ K. Finally, we add that the frequencies of $F = 22.2$ and 15.3 kT observed for $B \| [001]$ at a pressure of 29.5 kbar (Ref. 22) might be ascribed to the orbits Γ^e_{41} and Γ^e_{42}.

The quantitative agreement between experiment and theory [Fig. 6(b)] is however much worse than that for $LaRhSi_3$ (Fig. 2). In the first place, this can be attributed to that the large intra-atomic Coulomb interaction of the Ce $4f$ electrons cannot properly be dealt with by the local-density approximation. Improvement may be achieved by use of the LDA+U method with appropriate shift of the f level,[37] as has recently been applied to $CeIn_3$.[38] The truncation of the Fermi surface by the antiferromagnetic order would also have to be considered.

TABLE III. Calculated Fermi-surface parameters of $CeRhSi_3$.

Field direction	Calculation		
	Orbit[a]	F (kT)	m_{band}/m_e
[001]	Λ^h_{39}	0.96	4.83
	Λ^h_{39}	0.96	4.47
	Z^h_{39}	2.00	5.59
	Z^h_{40}	3.45	2.33
	W^h_{41}	7.07	2.68
	P^h_{41}	7.09	2.64
	P^h_{42}	8.25	2.37
	Γ^e_{42}	17.75	5.22
	Γ^e_{41}	23.20	14.28
[100]	F^h_{39}	0.41	5.79
	F^h_{39}	0.53	2.59
	F^h_{41}	2.28	5.52
	Z^h_{39}	2.70	4.27
	Z^h_{40}	3.21	3.30
	Σ^e_{42}	5.40	2.66
	F^h_{42}	5.76	6.66
	Z^h_{41}	6.32	3.51
	Z^h_{42}	7.15	2.77
[110]	U^h_{39}	1.90	5.43
	Z^h_{39}	2.01	3.74
	U^h_{39}	2.04	6.52
	U^h_{42}	2.82	3.63
	Z^h_{40}	3.33	4.48
	U^h_{41}	4.16	3.73
	U^h_{41}	4.21	3.29
	Δ^e_{42}	7.96	4.23
	Γ^e_{42}	8.38	5.08
	Γ^e_{41}	9.16	5.22

[a]The orbits are denoted by orbit center, band number, and orbit character, i.e., electron or hole.

IV. SUMMARY

We have performed angle-resolved dHvA measurements and FLAPW band-structure calculations for $LaRhSi_3$ and $CeRhSi_3$. The dHvA frequency branches observed in $LaRhSi_3$ can quantitatively be explained by the calculated Fermi surface, which consists of three pairs of inversion-asymmetry-split sheets. From the observed inversion-asymmetry splittings of the Fermi surface, the strength of the spin-orbit coupling is estimated to be of the order of 10^2 K, which is rather smaller than that reported for $LaIrSi_3$.[34] The

dHvA frequency branches observed in $CeRhSi_3$ are decidedly different from those in $LaRhSi_3$ and are difficult to explain with the $LaRhSi_3$ Fermi surface. This leads us to conclude that the Ce $4f$ electrons in $CeRhSi_3$ are itinerant, contributing to the Fermi surface, in the antiferromagnetic state, in line with our previous work.[21,22] The band-structure calculation assuming the itinerant Ce $4f$ electrons indicates that the electronic states near the Fermi level are mainly of Ce $4f$ character and yields the Fermi surface consisting two pairs of sheets. This calculated Fermi surface seems to provide plausible origins of some of the observed frequency branches, although the quantitative agreement between the experimental and the theoretical frequencies is poor.

ACKNOWLEDGMENTS

This work was supported by Grants-in-Aid for Scientific Research from the JSPS, Japan.

[1] N. Engel, H. F. Braun, and E. Parthé, J. Less-Common Met. **95**, 309 (1983).
[2] P. Lejay, I. Higashi, B. Chevalier, J. Etourneau, and P. Hagenmuller, Mater. Res. Bull. **19**, 115 (1984).
[3] P. Haen, P. Lejay, B. Chevalier, B. Lloret, J. Etourneau, and M. Sera, J. Less-Common Met. **110**, 321 (1985).
[4] Y. Muro, D. Eom, N. Takeda, and M. Ishikawa, J. Phys. Soc. Jpn. **67**, 3601 (1998).
[5] N. Aso, H. Miyano, H. Yoshizawa, N. Kimura, T. Komatsubara, and H. Aoki, J. Magn. Magn. Mater. **310**, 602 (2007).
[6] Y. Muro, M. Ishikawa, K. Hirota, Z. Hiroi, N. Takeda, N. Kimura, and H. Aoki, J. Phys. Soc. Jpn. **76**, 033706 (2007).
[7] N. Kimura, K. Ito, K. Saitoh, Y. Umeda, H. Aoki, and T. Terashima, Phys. Rev. Lett. **95**, 247004 (2005).
[8] N. Kimura, K. Ito, H. Aoki, S. Uji, and T. Terashima, Phys. Rev. Lett. **98**, 197001 (2007).
[9] N. Kimura, Y. Muro, and H. Aoki, J. Phys. Soc. Jpn. **76**, 051010 (2007).
[10] P. A. Frigeri, D. F. Agterberg, A. Koga, and M. Sigrist, Phys. Rev. Lett. **92**, 097001 (2004).
[11] M. Sigrist, D. Agterberg, P. Frigeri, N. Hayashi, R. Kaur, A. Koga, I. Milat, K. Wakabayashi, and Y. Yanase, J. Magn. Magn. Mater. **310**, 536 (2007).
[12] K. V. Samokhin, E. S. Zijlstra, and S. K. Bose, Phys. Rev. B **69**, 094514 (2004).
[13] I. A. Sergienko and S. H. Curnoe, Phys. Rev. B **70**, 214510 (2004).
[14] M. Oka, M. Ichioka, and K. Machida, Phys. Rev. B **73**, 214509 (2006).
[15] S. Fujimoto, J. Phys. Soc. Jpn. **75**, 083704 (2006).
[16] H. Tanaka, H. Kaneyasu, and Y. Hasegawa, J. Phys. Soc. Jpn. **76**, 024715 (2007).
[17] T. Yokoyama, S. Onari, and Y. Tanaka, Phys. Rev. B **75**, 172511 (2007).
[18] D. F. Agterberg and R. P. Kaur, Phys. Rev. B **75**, 064511 (2007).
[19] E. Bauer, G. Hilscher, H. Michor, C. Paul, E. W. Scheidt, A. Gribanov, Y. Seropegin, H. Noël, M. Sigrist, and P. Rogl, Phys. Rev. Lett. **92**, 027003 (2004).
[20] I. Sugitani, Y. Okuda, H. Shishido, T. Yamada, A. Thamizhavel, E. Yamamoto, T. D. Matsuda, Y. Haga, T. Takeuchi, R. Settai, and Y. Ōnuki, J. Phys. Soc. Jpn. **75**, 043703 (2006).
[21] N. Kimura, Y. Umeda, T. Asai, T. Terashima, and H. Aoki, Physica B **294-295**, 280 (2001), there was an error in the orientation of the used $LaRhSi_3$ sample. In Fig. 6 of this paper, read [100] and [001] as [001] and [100], respectively, and disregard the right half of the figure.
[22] T. Terashima, Y. Takahide, T. Matsumoto, S. Uji, N. Kimura, H. Aoki, and H. Harima, Phys. Rev. B **76**, 054506 (2007).
[23] H. Shishido, R. Settai, H. Harima, and Y. Ōnuki, J. Phys. Soc. Jpn. **74**, 1103 (2005).
[24] P. Coleman, C. Pépin, Q. Si, and R. Ramazashvili, J. Phys.: Condens. Matter **13**, R723 (2001).
[25] N. Harrison, U. Alver, R. G. Goodrich, I. Vekhter, J. L. Sarrao, P. G. Pagliuso, N. O. Moreno, L. Balicas, Z. Fisk, D. Hall, R. T. Macaluso, and J. Y. Chan, Phys. Rev. Lett. **93**, 186405 (2004).
[26] D. Shoenberg, *Magnetic Oscillations in Metals* (Cambridge University Press, Cambridge, 1984).
[27] A. Yanase, *Fortran Program for Space Group*, 1st ed. (Shokabo, Tokyo, 1985) (in Japanese).
[28] N. Harima, O. Sakai, T. Kasuya, and A. Yanase, Solid State Commun. **66**, 603 (1988).
[29] H. Harima and K. Takegahara, J. Magn. Magn. Mater. **272-276**, 475 (2004).
[30] Y. Muro, Ph.D. thesis, The University of Tokyo, 2000.
[31] T. Terashima, S. Uji, Y. Nagao, J. Yamaura, Z. Hiroi, and H. Harima, Phys. Rev. B **77**, 064509 (2008).
[32] V. P. Mineev and K. V. Samokhin, Phys. Rev. B **72**, 212504 (2005).
[33] E. I. Rashba, Sov. Phys. Solid State **2**, 1109 (1960).
[34] Y. Okuda, Y. Miyauchi, Y. Ida, Y. Takeda, C. Tonohiro, Y. Oduchi, T. Yamada, N. D. Dung, T. D. Matsuda, Y. Haga, T. Takeuchi, M. Hagiwara, K. Kindo, H. Harima, K. Sugiyama, R. Settai, and Y. Ōnuki, J. Phys. Soc. Jpn. **76**, 044708 (2007).
[35] A. Thamizhavel, H. Shishido, Y. Okuda, H. Harima, T. D. Matsuda, Y. Haga, R. Settai, and Y. Ōnuki, J. Phys. Soc. Jpn. **75**, 044711 (2006).
[36] T. Kawai, H. Muranaka, T. Endo, N. D. Dung, Y. Doi, S. Ikeda, T. D. Matsuda, Y. Haga, H. Harima, R. Settai, and Y. Ōnuki, J. Phys. Soc. Jpn. **77**, 064717 (2008).
[37] H. Harima, J. Magn. Magn. Mater. **226-230**, 83 (2001).
[38] M.-T. Suzuki and H. Harima, Physica B **403**, 1318 (2008).